Probabilistic Power Flow Analysis for Hybrid HVAC and LCC-VSC HVDC System

TONG SHU[1], (Student Member, IEEE), XINGYU LIN[1], (Student Member, IEEE), SUI PENG[2], XIAO DU[1], HUIXIANG CHEN[2], FENG LI[2], JUNJIE TANG[1], (Member, IEEE), AND WENYUAN LI[1], (Life Fellow, IEEE)

[1]State Key Laboratory of Power Transmission Equipment and System Security and New Technology, Power and Energy Reliability Research Center, Chongqing University, Chongqing 400044, China
[2]Grid Planning and Research Center, Guangdong Power Grid Corporation, China Southern Power Grid Company Limited, Guangzhou 510080, China

Corresponding author: Junjie Tang (tangjunjie@cqu.edu.cn)

ABSTRACT Some innovative works have been done to probabilistic power flow (PPF) analysis for hybrid HVAC and LCC-VSC HVDC system in this paper. Firstly, a unified method considering precise model of converters is proposed to solve a general deterministic power flow (DPF) calculation including hybrid LCC (Line Current Converter) and VSC (Voltage Source Converter), the pure VSC-MTDC (Voltage Source Converter-Multiple Terminal Direct Current) and pure LCC system. Meanwhile, with a large amount of renewable energy sources integrated to the main grid through DC grids, it will impose a stochastic impact on the secure operation of such hybrid AC/DC grids. Therefore, it becomes necessary to model the probabilistic uncertainties and analyze their effects on the operation of hybrid AC/DC systems under different control modes. Nevertheless, most power flow analysis methods for hybrid AC/DC system are still deterministic in nature. Therefore, a probabilistic method based on the combination of Nataf transformation and Latin hypercube sampling (LHS) is developed and proposed to solve this complex PPF problem in an efficient manner, which considers correlated various probabilistic uncertainties, e.g. wind speeds, solar radiations and loads following different types of probability distribution. Finally, the effectiveness of the unified DPF method is validated in a modified IEEE 14-bus system, while the proposed PPF is verified in a modified IEEE 118-bus system and the effects of uncertainties on the diverse operation modes of hybrid AC/DC grids are discussed as well.

INDEX TERMS Probabilistic power flow, hybrid AC/DC system, probabilistic uncertainty, droop control, renewable energy sources.

I. INTRODUCTION

With the increasing worldwide concerns on environmental pollution, global warming, energy and resources crisis, the topics on both smart grid and renewable energy generation have become very attractive most recently [1]. European Union (EU) has defined as a target for 2050 to reduce about 80%–95% of the greenhouse gas emissions compared to the levels in 1990 [2]. This implies that the penetration of renewable energy sources in future power system could be increased close to 100%. Nevertheless, how to integrate and transmit renewable energy in a high-efficiency and low-cost way is still a critical challenge. Meanwhile, High Voltage Direct Current (HVDC) is proved to be a preferable solution for addressing the renewable energy integration issue [3].

The associate editor coordinating the review of this manuscript and approving it for publication was Junjian Qi.

So far, there are two alternative mature types of HVDC technology available: LCC-HVDC (Line Current Converter based High Voltage Direct Current) and VSC-HVDC (Voltage Source Converter based High Voltage Direct Current), with pros and cons, individually [4], [5]. In order to make full use of their respective advantages, the hybrid AC/DC system incorporating both LCC and VSC attracts more attention recently [6], [7]. More importantly, the recent research reveals that the hybrid AC/DC system possess a fault self-cleaning capability [8].

One of the outstanding research issues lies in the steady-state behavior of the hybrid AC/DC system. The study of AC/DC power flow can be traced back to the 1950s [9]. In the past, numerous efforts have been spent on solving the AC/DC power flow based on LCC technology [10]–[13], and hence the power flow algorithm for such problem is getting quite mature. Unfortunately, the power loss of converters is

neglected in these researches. Recently, researchers start to focus on the power flow of VSC-MTDC (Voltage Source Converter-Multiple Terminal Direct Current). The algorithm is mainly improved from the following aspects: modeling of VSC-MTDC and solution techniques. In terms of modeling, literature [14] improves the convergence by decomposing the network into two building blocks: the DC grid and the AC grid with converter station. Literature [15] develops a redundant control structure called voltage margin control scheme, thus providing a backup DC slack converter in case that the main slack converter fails. Moreover, DC voltage control can be distributed over several converters using a voltage droop control [16]. In [17], filters are included in the model, but they are required to be loss-less; ad-hoc modifications are needed in the equations when transformer-less or filter-less operations are considered.

Regarding the solution techniques, the unified approach retains the strong convergence characteristics of NR (Newton-Raphson) method, but it is deemed as quite complex to program [9], [12], [18], [19]. The sequential solution method is easy to implement, as they enable the incorporation of MTDC systems into existing AC power flow software [20], [21]. However, the convergence of sequential method is poor, thus the third-order and sixth-order Newton-type method have been suggested to improve the efficiency of such algorithms [22]. Although the power flow considering pure LCC or pure VSC system has been mature, individually, there are still existing different models and governing equations of LCC and VSC converter stations. Therefore, only a few studies have been directed towards the more practical power flow analysis of hybrid AC/DC system incorporating both LCC and VSC.

With a significant amount of volatile renewable energy sources integrating into the hybrid AC/DC grids, it has brought about new challenges to the stable operation of hybrid AC/DC grids due to its strong uncertainties. Studying the impact of uncertainties is important for power system operation and planning. The deterministic power flow (DPF) lacks an ability to recognize the probabilistic essence of uncertainty sources. Accordingly, the probabilistic power flow (PPF) proposed by Borkowska in 1974 [23] is an essential approach to explore the steady-state characteristics of hybrid AC/DC grids with various types of possible uncertainties, such as wind speeds, solar radiations and loads. Literature [24], [25] pave the way for the field of probabilistic power flow for AC/DC grids. However, the droop control, the precise model of converter and LCC converter are not considered in these researches. To the best knowledge of authors, the study on the application of PPF to hybrid HVAC and LCC-VSC HVDC system is still not accessible in the published literatures so far.

In general, PPF methods can be mainly divided into three categories: analytical methods, approximate methods and Monte Carlo Simulation (MCS) method. These analytical methods are computationally efficient, but it suffers from some mathematic manipulations, such as linearization and

independence which are usually made to simplify the original problem [26]. The point estimate method (PEM) [27] and the unscented transformation (UT) [28] represent the typical approximate methods, which are efficient but at the price of accuracy loss, as well they can only obtain the accurate low-order statistical moments of target random output variables. On the contrary, the MCS is able to handle complex PPF problems without simplification and solve the problem via repetitive DPF calculation. Actually, the MCS is widely recognized as the standard reference for checking the accuracy of other methods. However, MCS itself requires numerous simulations to reach an acceptable accuracy, which falls into a heavy burden in computation. Therefore, some improved sampling techniques, such as Latin hypercube sampling (LHS), have been introduced to further boost the sampling efficiency [29], [30], which are expected to keep a better balance between accuracy and efficiency particularly for the complex PPF on hybrid AC/DC grid.

In order to address the deficiency issues mentioned above, a new probabilistic power flow analysis for hybrid AC/DC system is proposed in this paper. The major contributions cover the followings:

1) A unified deterministic power flow algorithm for hybrid HVAC and LCC-VSC HVDC system with considering coordinated control is proposed in this paper, in which the precise model of converter is considered as well. This facilitates the power flow calculation for various control modes, arbitrary topologies and different types of converter station in such hybrid AC/DC grids. The performance is validated via a general comparison to the sequential method.
2) The PPF analysis particular for hybrid HVAC and LCC-VSC HVDC system, based on the combination of LHS and Nataf transformation, is correspondingly presented for the first time, with a good accuracy, efficiency and robustness.
3) The impacts of various uncertainty sources considering correlation on different control modes and operation for the hybrid HVAC and LCC-VSC HVDC system are investigated and discussed comprehensively.

The remainder of this paper is organized as follows. The power flow modeling of hybrid AC/DC system is introduced in Section II, the coordinated control scheme for hybrid HVDC system is presented in Section III, and the unified power flow algorithm is proposed in Section IV. Accordingly, the PPF framework for hybrid AC/DC is demonstrated in Section V. A set of case studies are provided in Section VI, based on which the conclusions are drawn in Section VII.

II. STEADY-STATE MODELING OF A HYBRID AC/DC SYSTEM

A. VSC STATION MODELING
Fig. 1 illustrates the structure of VSC station. The AC grid connects the VSC bus via a transformer, a filter and a reactor, while the DC bus is connected to the DC side of VSC station.
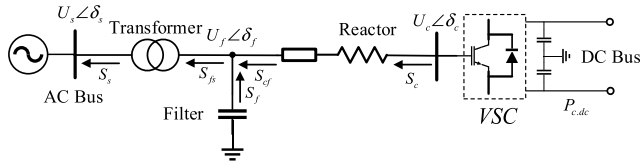
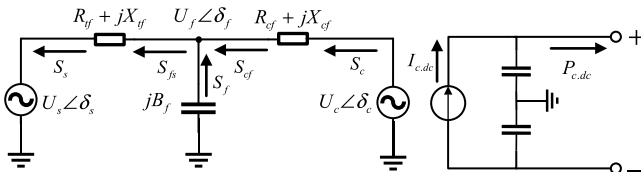**FIGURE 1.** Diagram for the structure of VSC station.

FIGURE 2. Equivalent circuit diagram of a VSC station.

FIGURE 3. Diagram for the structure of LCC station.

The equivalent circuit diagram of the VSC station is illustrated in Fig. 2. The AC side and DC side of VSC are modeled by an equivalent voltage source and an equivalent current source, respectively. The transformer is represented by an impedance $Z_t = R_{tf} + jX_{tf}$, i.e. the corresponding admittance $G_{tf} + jB_{tf} = 1/Z_t$. The rector impedance is $Z_c = R_{cf} + jX_{cf}$, with $G_{cf} + jB_{cf} = 1/Z_c$. Corresponding filter susceptance is jB_f. $U_s\angle\delta_s$ is the AC bus voltage phasor and $U_f\angle\delta_f$ represents the voltage phasor of filter node. $U_c\angle\delta_c$ denotes the VSC bus voltage phasor.

Thus, the equations for power flowing to the AC network can be written as:

$$P_s = -U_s^2 G_{tf} + U_s U_f[G_{tf}\cos(\delta_s-\delta_f)+B_{tf}\sin(\delta_s-\delta_f)] \quad (1)$$
$$Q_s = U_s^2 B_{tf} + U_s U_f[G_{tf}\sin(\delta_s-\delta_f)-B_{tf}\cos(\delta_s-\delta_f)] \quad (2)$$

The complex power at the VSC converter side can be determined by:

$$P_c = U_c^2 G_{cf} - U_c U_f[G_{cf}\cos(\delta_f-\delta_c)-B_{cf}\sin(\delta_f-\delta_c)] \quad (3)$$
$$Q_c = -U_c^2 B_{cf} + U_c U_f[G_{cf}\sin(\delta_f-\delta_c)+B_{cf}\cos(\delta_f-\delta_c)] \quad (4)$$

Assuming the AC filters to be lossless, the injected complex power of filter can be simplified to only remain its reactive power.

$$Q_f = -U_f^2 B_f \quad (5)$$

While the expressions for the complex power flowing of filter side through the transformers are written as:

$$P_{sf} = U_f^2 G_{tf} - U_f U_s[G_{tf}\cos(\delta_s-\delta_f)-B_{tf}\sin(\delta_s-\delta_f)] \quad (6)$$
$$Q_{sf} = -U_f^2 B_{tf} + U_f U_s[G_{tf}\sin(\delta_s-\delta_f)+B_{tf}\cos(\delta_s-\delta_f)] \quad (7)$$

Similarly, the corresponding equations for the power flowing to the phase reactor side can be given below:

$$P_{cf} = -U_f^2 G_{cf} + U_f U_c[G_{cf}\cos(\delta_f-\delta_c)+B_{cf}\sin(\delta_f-\delta_c)] \quad (8)$$
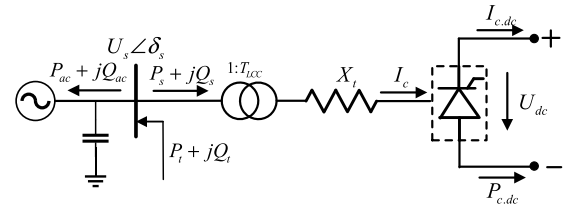$$Q_{cf} = U_f^2 B_{cf} + U_f U_c[G_{cf}\sin(\delta_f-\delta_c)-B_{cf}\cos(\delta_f-\delta_c)] \quad (9)$$

The detailed converter loss model is employed in this paper, via using a generalized active power loss formula that the converter loss is quadratically dependent on the converter current I_c:

$$P_{c.loss} = a|I_c|^2 + b|I_c| + c \quad (10)$$

where a, b, c are the coefficients derived from practical project, and I_c can be calculated in advance according to the following equation.

$$I_c = (U_f e^{j\delta_f} - U_c e^{j\delta_c})(G_{cf} + jB_{cf}) \quad (11)$$

From the DC side of VSC, $P_{c.dc}$ is the injected power from the VSC side to DC grid. With the power flow direction defined in Fig. 1, $P_{c.dc}$ can be deduced as:

$$P_{c.dc} = -P_c - P_{c.loss} \quad (12)$$

B. LCC STATION MODELING
Fig. 3 illustrates the structure of a LCC station. The DC grid utilizes bipolar transmission. In Fig. 3, U_{dc} and $I_{c.dc}$ are the DC voltage and DC current, respectively. I_c is the fundamental AC current injected into the converter, and T_{LCC} is the transformer turns ratio. $U_s\angle\delta_s$ is the AC bus voltage phasor while X_t is the converter reactance.

The DC equations of the LCC station are given as below:

$$U_{dc} = \frac{3\sqrt{2}}{\pi}n_{ti}T_{LCC}U_s\cos\theta - \frac{3}{\pi}n_{ti}X_t I_{c.dc}sign \quad (13)$$

$$U_{dc} = \frac{3\sqrt{2}}{\pi}k_\gamma n_{ti}T_{LCC}U_s\cos\varphi \quad (14)$$

$$I_c = \frac{\sqrt{6}}{\pi}k_\gamma n_{ti}I_{c.dc} \quad (15)$$

where n_{ti} represents the number of converter bridge, θ is the converter commutation angle (i.e. rectifier commutation angle or inverter extinct angle); φ is the converter power factor angle; *sign* denotes the station type (i.e. $+1$ for rectifier and -1 for inverter). When the commutation is taken into consideration, $k_\gamma = 0.995$.

Considering the precise converter loss in the LCC station, it can be modeled by a second-order polynomial:

$$P_{c.loss} = a|I_c|^2 + b|I_c| + c \quad (16)$$

$$I_c = \frac{\sqrt{6}}{\pi}k_\gamma n_{ti}I_{c.dc} \quad (17)$$

where a, b, c are the coefficients derived from practical project, and I_c can be calculated according to equation (17).

The complex power $S_s = P_s + jQ_s$ injected from the AC grid to LCC station can be expressed as (18) and (19), where $P_{c.dc}$ is the active power that the LCC station injects into the DC grid.

$$P_s = P_{c.dc} + P_{c.loss} \tag{18}$$

$$Q_s = P_s \tan\varphi sign \tag{19}$$

$$P_{c.dc} = U_{dc}I_{c.dc} \tag{20}$$

C. DC NETWORK MODELING

The DC network is consist of the DC power sources, DC loads, DC transmission lines and equivalent station model; while the structure diagram and corresponding power flow equations can be referred to literature [19].

III. CONTROL SCHEME OF HYBRID HVDC SYSTEM

For the stable operation of the DC grid, it is essential to maintain the power balance and the DC voltage in a normal range. The control modes of HVDC system can be usually divided into three categories, including master-slave control, voltage margin control and voltage droop control [19].

A. CONTROL SCHEME OF HYBRID HVDC SYSTEM

The control schemes for pure LCC and pure VSC can be accessible in [13] and [19], respectively. Considering the different operational characteristics between the LCC and VSC station, a unified expression for hybrid LCC-VSC HVDC system with covering different control modes and different converter types is proposed herein. For a hybrid LCC-VSC HVDC system, D-axis control will impose a denominating influence on the overall DC system power balance and voltage stability. Correspondingly, the unified expressions for D-axis control equations can be deduced and written as below.

$$\Delta D = K_{Ps}(P_s - P_s^*) + K_{Udc}(U_{dc} - U_{dc}^*)$$
$$+ K_{Pdc}(P_{dc} - P_{dc}^*) + K_{Idc}(I_{dc} - I_{dc}^*) = 0 \tag{21}$$

where the superscript $*$ indicates the reference value for corresponding parameters. K_{Ps}, K_{Udc}, K_{Pdc}, K_{Idc} are the weight coefficients for AC active power, DC voltage, DC active power and DC current. The weight coefficients of the corresponding control schemes utilized herein are summarized in TABLE 1.

According to the D-axis control scheme, the DC nodes can be divided into three major types:

I) Nodes connected to the LCC stations with constant power P_{dc} control or constant current I_{dc} control, and VSC stations with constant P_s control. (i.e. power station)

II) Nodes connected to the LCC stations and VSC stations with constant U_{dc} control. (i.e. voltage station)

III) Nodes connected to VSC stations with $U_{dc} - P_{dc}$ droop control or $U_{dc} - I_{dc}$ control. (i.e. droop station)

There is at least one type **II** or **III** node, and at most one type **II** node in a hybrid HVDC system. Usually, a hybrid HVDC has one type **II** node and several type **I** nodes, or at least one type **III** node and several type **I** nodes.

TABLE 1. Weight coefficients for D-Axis control modes of hybrid HVDC.

D-axis control	K_{Ps}	K_{Udc}	K_{Pdc}	K_{Idc}
Constant P_s	1	0	0	0
Constant U_{dc}	0	1	0	0
Constant P_{dc}	0	0	1	0
Constant I_{dc}	0	0	0	1
$U_{dc} - P_{dc}$ Droop	0	1	$\neq 0$	0
$U_{dc} - I_{dc}$ Droop	0	1	0	$\neq 0$

TABLE 2. Weight coefficients for hybrid HVDC E/Q-Axis control modes.

E-axis control	K_T	K_θ	Q-axis control	K_{Qs}	K_{Uac}
Constant T_{LCC}	1	0	Constant Q_s	1	0
Constant θ	0	1	Constant U_{ac}	0	1

For remainder of LCC and VSC controls, the transformer ratio T_{LCC} and converter control angle θ are treated as E-axis control variables for LCC converter. Regarding VSC converter, the Q-axis ones include the injected reactive power from AC to VSC station Q_s and AC voltage U_{ac}.

$$\Delta E_{LCC} = K_T(T_{LCC} - T_{LCC}^*) + K_\theta(\cos\theta - \cos\theta^*) = 0 \tag{22}$$

$$\Delta Q_{VSC} = K_{Qs}(Q_s - Q_s^*) + K_{Uac}(U_{ac} - U_{ac}^*) = 0 \tag{23}$$

where K_T, K_θ, K_{Qs}, K_{Uac} are the weight coefficients for transformer ratio, converter control angle, AC reactive power, and AC voltage, individually. Correspondingly, there must be one non-zero weight coefficient in each control equation, as shown in TABLE 2.

IV. PROPOSED UNIFIED POWER FLOW ALGORITHM

The Newton-Raphson (NR) method used in steady-state power flow analysis works based on the Taylor's series expansion. To apply the NR method to solve power flow calculation, the AC bus voltages are normally expressed in a polar form. In order to analyze and calculate conveniently, a set of compact mismatch equations consisting of the AC equations $F_{AC}(X)$, VSC equations $F_{VSC}(X)$, LCC equations $F_{LCC}(X)$ and DC equations $F_{DC}(X)$ are defined generally as below.

$$F(X) = [F_{AC}(X)^T, F_{VSC}(X)^T, F_{LCC}(X)^T, F_{DC}(X)^T]^T = 0 \tag{24}$$

where $F(X)$ represents the nonlinear function vector of mismatch equations; X is the vector of state variables, including four major parts $X = [X_{AC}^T, X_{VSC}^T, X_{LCC}^T, X_{DC}^T]^T$, which are

defined with more details as follows.

$$\begin{cases} X_{AC} = [\delta^T, U^T]^T \\ X_{VSC} = [\delta_f^T, U_f^T, \delta_c^T, U_c^T, P_{c.dc}^T]^T \\ X_{LCC} = [P_{c.dc}^T, cos\theta^T, T_{LCC}^T]^T \\ X_{DC} = [U_{dc}^T]^T \end{cases} \quad (25)$$

where δ is the column vector of power angles, U is the column vector of PQ node voltage amplitudes in AC grid, δ_f and U_f are the voltage angles and magnitudes respectively of all VSC filter buses, while δ_c and U_c are the voltage angles and magnitudes, respectively, of all VSC buses. $P_{c.dc}$ denotes the injected active power from the converter station side into DC grid. $cos\theta$ and T_{LCC} are the control angle and transformer ratios of the LCC station, respectively. U_{dc} contains the voltage magnitudes of all the DC buses.

A. MISMATCH EQUATIONS OF AC GRID

It is assumed that there are n_{ac} AC nodes in AC grid, including one slack bus, n_{PQ} PQ bus nodes and n_{PV} PV bus nodes. The active and reactive power injected at arbitrary bus i are defined and explained in [31], which can be calculated as:

$$\begin{cases} P_{ac,i}(U, \delta) = U_i \sum_{j=1}^{n_{ac}} U_j(G_{ij}\cos\delta_{ij} + B_{ij}\sin\delta_{ij}) \\ Q_{ac,i}(U, \delta) = U_i \sum_{j=1}^{n_{ac}} U_j(G_{ij}\sin\delta_{ij} - B_{ij}\cos\delta_{ij}) \end{cases} \quad (26)$$

The power balance equations for arbitrary bus i can be expressed:

$$\begin{cases} \Delta P_{ac,i} = P_{Gac,i} + P_{Conac,i} - P_{Lac,i} - P_{ac,i}(U, \delta) \\ \Delta Q_{ac,i} = Q_{Gac,i} + Q_{Conac,i} - Q_{Lac,i} - Q_{ac,i}(U, \delta) \end{cases} \quad (27)$$

The two equations above involve the terms $P_{Conac,i}$, Q_{conaci} for the purpose of generalization. Obviously, the buses that are not connected to the LCC or VSC converter will have these terms setting to zero as shown below.

$$P_{Conac,i} = \begin{cases} P_{s,i}, \text{ connected to a VSC station} \\ 0, \text{ non-connected to converter station} \\ -P_{s,i}, \text{ connected to a LCC station} \end{cases} \quad (28)$$

$$Q_{Conac,i} = \begin{cases} Q_{s,i}, \text{ connected to a VSC station} \\ 0, \text{ non-connected to converter station} \\ -Q_{s,i}, \text{ connected to a LCC station} \end{cases} \quad (29)$$

where $P_{Gac,i}$ and $Q_{Gac,i}$ are the active and reactive generation power, respectively. $P_{Lac,i}$ and $Q_{Lac,i}$ are the corresponding active and reactive load power. Hence, the mismatch equations of AC grids can be written as

$$F_{AC}(X) = [\Delta P^T, \Delta Q^T]^T = 0 \quad (30)$$

where $(n_{ac} - 1)$ dimensional column vector ΔP is formed by active power $\Delta P = [\Delta P_1, \Delta P_2, \dots, \Delta P_{n_{ac}-1}]^T$ of PV and PQ node, $(n_{ac} - n_{PV} - 1)$ dimensional column vector ΔQ is formed by reactive power $\Delta Q = [\Delta Q_1, \Delta Q_2, \dots, \Delta Q_{n_{ac}-n_{PV}-1}]^T$ of PQ node.

B. MISMATCH EQUATIONS OF THE VSC STATION

There are two basic active and reactive power mismatch equations at the filter bus, which can be expressed as:

$$\Delta P_{fi} = P_{cfi} - P_{fsi} = 0 \quad (31)$$
$$\Delta Q_{fi} = Q_{cfi} - Q_{fsi} - Q_{fi} = 0 \quad (32)$$

In order to match the number of equations and variables, it needs two additional equations for solving the power flow calculation of VSC station. According to the control modes of VSC, D-axis mismatch equation and Q-axis mismatch equation are available, respectively.

$$\Delta D_{mismatch,i}$$
$$= \begin{cases} \Delta P_{si} = P_{si} - P_{si}^{ref} = 0 \\ \Delta U_{dci} = U_{dci} - U_{dci}^{ref} = 0 \\ \Delta f_{U-P,droop,i} = U_{dci} \\ \quad - U_{dcrefi} - K_{U-P,i}(P_{dci} - P_{dcrefi}) = 0 \\ \Delta f_{U-I,droop,i} = U_{dci} \\ \quad - U_{dcrefi} - K_{U-I,i}(\frac{P_{dci}}{U_{dci}} - \frac{P_{dcrefi}}{U_{dcrefi}}) = 0 \end{cases} \quad (33)$$

The corresponding D-axis control mismatch equations are shown as above, in which K_{U-P} and K_{U-I} are droop coefficient for $U_{dc} - P_{dc}$ droop and $U_{dc} - I_{dc}$ control, respectively. In practical calculation, only one D-axis mismatch equation needs to be chosen according to the control mode. In particular, once droop control is applied, beside from the D-axis droop control equations, there must be adding another equation.

$$\Delta P_{exchange} = P_{c,dc} + P_{c.loss} + P_{ci} = 0 \quad (34)$$

Accordingly, the Q-axis control mismatch equations can be written as below.

$$\Delta Q_{mismatch,i} = \begin{cases} \Delta Q_{si} = Q_{si} - Q_{si}^{ref} = 0 \\ \Delta U_{aci} = U_{aci} - U_{aci}^{ref} = 0 \end{cases} \quad (35)$$

Similar to D-axis, one Q-axis mismatch equation needs to be chosen according to the control mode.

It is assumed that VSC stations contain n_{VSC} nodes, with n_{droop} nodes using droop control. Then, the mismatch equations of all VSC stations are defined as:

$$F_{VSC}(X)$$
$$= [\Delta P_f^T, \Delta Q_f^T, \Delta D_{mismatch}^T, \Delta P_{exchange}^T, \Delta Q_{mismatch}^T]^T \quad (36)$$

where all vectors of the mismatch equations have n_{VSC} elements, in particular $\Delta P_{exchange}$ will appear only when the droop control is adopted. Thus, the injected active power $\Delta P_{exchange} = [\Delta P_{exchange,1}, \Delta P_{exchange,2}, \dots, \Delta P_{exchange,n_{droop}}]^T$ from the VSC to DC grid can be determined.

C. MISMATCH EQUATIONS OF THE LCC STATION

The basic equation of LCC station can be expressed as:

$$\Delta d_{1i} = U_{dci} - \frac{3\sqrt{2}}{\pi} n_{ti} T_{LCCi} U_{si} \cos \theta_i + \frac{3}{\pi} n_{ti} X_t I_{c,dc} sign \tag{37}$$

Similar to the VSC station, D-axis and E-axis mismatch equations are added to solve the power flow calculation.

$$\Delta D_{LCC-mismatch,i} = \begin{cases} \Delta P_{dci} = P_{dci} - P_{dci}^* = 0 \\ \Delta I_{dci} = I_{dci} - I_{dci}^* = 0 \\ \Delta U_{dci} = U_{dci} - U_{dci}^* = 0 \end{cases} \tag{38}$$

In practical calculation, only one D-axis mismatch equation needs to be chosen according to the control mode. Besides, there is another power equation required in the calculation.

$$P_{dci} = U_{dci} I_{dci} \tag{39}$$

Then the E-axis mismatch equation can be represented.

$$\Delta E_{LCC-mismatch,i} = \begin{cases} \Delta T_{LCCi} = T_{LCCi} - T_{LCCi}^* = 0 \\ \Delta \cos \theta_i = \cos \theta_i - \cos \theta_i^* = 0 \end{cases} \tag{40}$$

The mismatch equations of all LCC stations are defined as follows.

$$\boldsymbol{F}_{LCC}(\boldsymbol{X}) = [\Delta d_1^T, \Delta D_{LCC-mismatch}^T, \Delta E_{LCC-mismatch}^T]^T \tag{41}$$

where all the vectors relevant to the mismatch equations totally have n_{LCC} elements.

D. MISMATCH EQUATIONS OF THE DC GRID

According to the power balance of the DC bus, the following equation can be obtained.

$$\Delta P_{dci} = P_{Gdci} + P_{converter-DC,i} - P_{Ldci}$$
$$- \sum_{j=1}^{n} Y_{dcij} U_{dcj} U_{dci} = 0 \tag{42}$$

Similar to AC grid, buses that are not connected to the LCC or VSC converter will have $P_{converter-DC,i}$ as zero, which is shown below.

$$P_{converter-DC,i}$$
$$= \begin{cases} P_{c.dci} & connected\ to\ LCC\ or\ VSC\ station \\ 0 & non-connected\ to\ converter\ station \end{cases} \tag{43}$$

where P_{Gdci} and P_{Ldci} are the active generation power and load power, respectively. Thus, the mismatch equations of DC grid can be expressed as:

$$\boldsymbol{F}_{DC}(\boldsymbol{X}) = [\Delta \boldsymbol{P}_{dc}^T]^T \tag{44}$$

where $\Delta \boldsymbol{P}_{dc} = [\Delta P_{dc1}, \Delta P_{dc2}, \dots, \Delta P_{dcn_{dc}}]^T$.

E. AN UNIFIED SOLUTION ALGORITHM

The unified iterative power flow calculation algorithm for hybrid AC/DC is proposed herein. The criterion for power flow convergence is defined as:

$$\max(\boldsymbol{F}(\boldsymbol{X})) < \varepsilon \tag{45}$$

where ε stands for the accuracy of the convergence. Usually, $\varepsilon = 10^{-5}$ can be set.

1) NR ITERATION METHOD

To apply the NR method to solve the power flow of hybrid AC/DC grid, neglecting the high-order terms, the Taylor series expansion of (24) can be formed as below.

$$\begin{bmatrix} \boldsymbol{F}_{AC} \\ \boldsymbol{F}_{VSC} \\ \boldsymbol{F}_{LCC} \\ \boldsymbol{F}_{DC} \end{bmatrix} = - \begin{bmatrix} \frac{\partial \boldsymbol{F}_{AC}}{\partial \boldsymbol{X}_{AC}} & \frac{\partial \boldsymbol{F}_{AC}}{\partial \boldsymbol{X}_{VSC}} & \frac{\partial \boldsymbol{F}_{AC}}{\partial \boldsymbol{X}_{LCC}} & 0 \\ \frac{\partial \boldsymbol{F}_{VSC}}{\partial \boldsymbol{X}_{AC}} & \frac{\partial \boldsymbol{F}_{VSC}}{\partial \boldsymbol{X}_{VSC}} & 0 & \frac{\partial \boldsymbol{F}_{VSC}}{\partial \boldsymbol{X}_{DC}} \\ \frac{\partial \boldsymbol{F}_{LCC}}{\partial \boldsymbol{X}_{AC}} & 0 & \frac{\partial \boldsymbol{F}_{LCC}}{\partial \boldsymbol{X}_{LCC}} & \frac{\partial \boldsymbol{F}_{LCC}}{\partial \boldsymbol{X}_{DC}} \\ 0 & \frac{\partial \boldsymbol{F}_{DC}}{\partial \boldsymbol{X}_{VSC}} & \frac{\partial \boldsymbol{F}_{DC}}{\partial \boldsymbol{X}_{LCC}} & \frac{\partial \boldsymbol{F}_{DC}}{\partial \boldsymbol{X}_{DC}} \end{bmatrix}$$
$$\times \begin{bmatrix} \boldsymbol{X}_{AC} \\ \boldsymbol{X}_{VSC} \\ \boldsymbol{X}_{LCC} \\ \boldsymbol{X}_{DC} \end{bmatrix} \tag{46}$$

In order to analyze and calculate conveniently, the unified power flow model of hybrid AC/DC grid can be expressed in a compact manner as:

$$\boldsymbol{F}(\boldsymbol{X}) = -\boldsymbol{J}\Delta\boldsymbol{X} \tag{47}$$

According to the NR iteration method, these variable corrections can be calculated.

$$\Delta \boldsymbol{X} = -\boldsymbol{J}^{-1}\boldsymbol{F}(\boldsymbol{X}) \tag{48}$$

2) LIMIT CHECK AND CONTROL MODES SWITCHING

For the ith VSC station with rated apparent power S_{Ni}, the active power P_{si} and the reactive power Q_{si} should satisfy such inequality below.

$$P_{si}^2 + Q_{si}^2 \leq S_{Ni}^2 \tag{49}$$

After the convergence, the limit of Q_{si} is

$$Q_{s\max i} = \sqrt{S_{Ni}^2 - P_{si}^2} \tag{50}$$

If $|Q_{si}| \leq Q_{s\max i}$ satisfies, the DPF calculation is valid. However, if $|Q_{si}| > Q_{s\max i}$, the Q-axis control mode should be modified from constant U_{si} to constant Q_{si} with $Q_{si}^* = \pm Q_{s\max i}$. Accordingly, the DPF calculation needs to be restarted.

For the ith LCC station with constant T_{LCC} control, when the state variable $\cos\theta \geq 1$ during calculating procedure, T_{LCC} should be relaxed as a state variable, and the value of $\cos\theta$ is replaced by its value in the last iteration or a specific

preset value. Meanwhile, to obtain the discrete integer value of T_{LCC}, it is regulated to the closest gear as follows:

$$\Delta T_{LCCi} = \left\lceil \Delta T'_{LCCi}/T_{step} \right\rceil \times T_{step} \tag{51}$$

where ΔT_{LCCi} is the actual correction value, $\lceil \ \rceil$ denotes the ceiling function, $\Delta T'_{LCCi}$ is the calculated value, and T_{step} represents the step of tap changer of the converter transformer.

V. THE PPF FRAMEWORK OF HYBRID AC/DC GRIDS

The fundamental idea of the PPF is to obtain the probabilistic characteristics, such as means and variances, of target output variables by conducting DPF calculation according to the given distribution of the input variables. In this section, the approach based on the combination of LHS and Nataf transformation is developed in particular to solve the PPF calculation for hybrid AC/DC grids.

A. NATAF TRANSFORMATION

Nataf transformation is a powerful tool to establish the relationship between correlated input random variables following any distribution and those following normal distribution, thus for a general probabilistic modeling in the scope of Pearson correlation. The basic principles of Nataf transformation are described in what follows.

Generally, the random input variables in PPF of hybrid AC/DC grid include wind speed, solar radiation, load and so forth, which can be denoted by a K-dimensional vector $\boldsymbol{R} = [R_1, R_2, \ldots, R_K]^T$ with the correlation matrix $\boldsymbol{C_R}$.

$$\boldsymbol{C_R} = \begin{bmatrix} 1 & \rho_{12} & \cdots & \rho_{1K} \\ \rho_{21} & 1 & \cdots & \rho_{2K} \\ \vdots & \vdots & \ddots & \vdots \\ \rho_{K1} & \rho_{K2} & \cdots & 1 \end{bmatrix}, \rho_R(i,j) = \frac{cov(R_i, R_j)}{\sigma_i \sigma_j} \tag{52}$$

where $\rho_R(i,j)$ and $cov(R_i, R_j)$ are the correlation and covariance of R_i and R_j, respectively; and σ_i and σ_j are standard deviations (STDs) of R_i and R_j. By applying the inverse transformation method, the original random vector $\boldsymbol{R}$ can be transferred to a standard normal vector $\boldsymbol{Z}$, as shown below.

$$\boldsymbol{Z} = [\Phi^{-1}[F_1(R_1)], \Phi^{-1}[F_2(R_2)], \ldots, \Phi^{-1}[F_K(R_K)]]^T \tag{53}$$

where $\Phi(\cdot)$ denotes the single-variable standard normal cumulative distribution function (CDF) of $\boldsymbol{Z}$; and F_k is the CDF of R_k. $\rho_Z(i,j)$ represents the correlation coefficient between Z_i and Z_j. According to Nataf transformation, the relationship between each pair $\rho_R(i,j)$ and $\rho_Z(i,j)$ can be written as:

$$\rho_R(i,j)$$
$$= \frac{\int\limits_{-\infty}^{+\infty}\int\limits_{-\infty}^{+\infty} F_i^{-1}[\Phi(Z_i)]F_j^{-1}[\Phi(Z_j)]\varphi_{\rho_Z(i,j)}(z_i, z_j)dz_i dz_j - \mu_i \mu_j}{\sigma_i \sigma_j} \tag{54}$$

where $\mu_i(\mu_j)$ and $\sigma_i(\sigma_j)$ are the mean and STD of $R_i(R_j)$; and $\varphi(z_i, z_j, \rho_Z)$ is the joint PDF of the bivariate standard normal distribution, given by

$$\varphi_{\rho_Z(i,j)}(z_i, z_j) = \frac{1}{2\pi\sqrt{1-\rho_Z^2}} \exp\left(\frac{-(z_i^2 - 2\rho_Z z_i z_j + z_j^2)}{2(1-\rho_Z^2)}\right) \tag{55}$$

Seen from equations (54) and (55), although $\rho_Z(i,j)$ can be hardly expressed by $\rho_R(i,j)$ in an explicit form, $\rho_Z(i,j)$ can be obtained with satisfied precision according to $\rho_R(i,j)$ by an efficient method in [32]. After calculating each correlation coefficient, individually, a symmetric matrix $\boldsymbol{C_Z}$ is determined. Correspondingly, it will be used in combination with LHS sampling technique for generating the samples of uncorrelated standard normal distributions, correlated standard normal distributions and correlated original arbitrary distributions, successively.

B. PROCEDURE FOR SOLVING THE PPF OF HYBRID AC/DC GRIDS BASED ON THE COMBINATION OF LHS AND NATAF TRANSFORMATION

The procedure for solving the PPF of hybrid AC/DC grids with correlated wind speeds, solar radiation, and loads following different distributions can be summarized and presented as follows:

Step 1. Input the control modes and original model parameters of hybrid AC/DC grids, and obtain the probability distributions of all the random input variables; then, get the Pearson correlation coefficient matrix $\boldsymbol{C_R}$ and the corresponding CDF's inverse function $\boldsymbol{F^{-1}}$.

Step 2. Transform the $\boldsymbol{C_R}$ into standard Gaussian scope to obtain $\boldsymbol{C_Z}$ by means of Nataf transformation, and then calculate the lower triangle matrix $\boldsymbol{L}$ from $\boldsymbol{C_Z}$ with a Cholesky decomposition.

Step 3. Generate the $K \times N$ sample matrix $\boldsymbol{H}$ by sampling the K independent standard normal random variables with a size of N based on LHS [30].

Step 4. Build normal distribution matrix $\boldsymbol{Z} = \boldsymbol{LH}$ whose correlation matrix of each column is $\boldsymbol{C_Z}$.

Step 5. Transform the standard Gaussian samples $\boldsymbol{Z}$ into the original random space by means of the inverse transformation $\boldsymbol{R} = \boldsymbol{F^{-1}}(\boldsymbol{Z})$.

Step 6. Feed the samples in the original random space to the DPF model (46) of hybrid AC/DC grids and finish the calculation one by one. Obtain the statistics (e.g. means, STDs, CDF and PDF) of the random output variables (e.g. bus voltage magnitude, phase angle, branch flow, control parameter and so on).

VI. CASE STUDY
A. PERFORMANCE ASSESSMENT OF THE PROPOSED HYBRID AC/DC DPF ALGORITHM
The performance of the proposed DPF model is assessed using a modified IEEE 14-bus system firstly. As shown
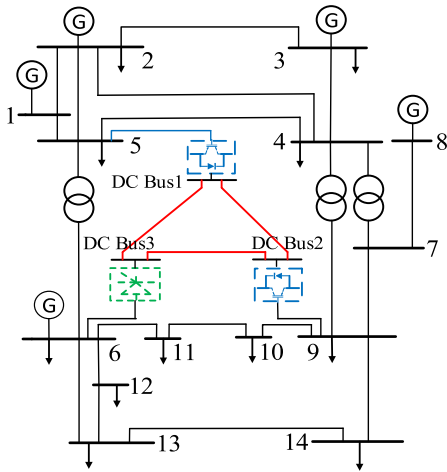
FIGURE 4. Modified IEEE 14-bus system with hybrid AC/DC grid incorporating both LCC and VSC.

TABLE 3. The resistance of DC lines.

	L_{12}	L_{13}	L_{23}
Resistance/p.u.	0.02	0.05	0.008

TABLE 4. The parameters of converter station.

Station(VSC)	Z_t /p.u.	Z_c /p.u.	B_f /p.u.	a, b, c / 10^{-3}
1	0.003+0.1j	0.15j	0	1, 4, 8
2	0.003+0.1j	0.15j	0	1, 4, 8
Station(LCC)	X_c /p.u.			a, b, c / 10^{-3}
3	0.15			0.25, 0.5, 1

in Fig. 4, an extra three-terminal DC grid incorporating LCC and VSC is added as the DC model. The base power of hybrid AC/DC system is set to be 100 MVA. The base voltage of AC grid is 220 kV, and the base voltage of DC grid is ± 200 kV. Note that the subsequent calculation is implemented in MATLAB with an Inter (R) Core (TM) i5-6500 CPU @ 3.20 GHz and 16GB of RAM memory.

The corresponding parameters of the DC model are given in TABLE 3 and TABLE 4.

1) VALIDITY OF THE PROPOSED DPF ALGORITHM

In order to validate the effectiveness and feasibility of the proposed unified power flow algorithm in particular for the new hybrid AC/DC system, a sequential iteration method is used for a comparison. The master-slave control scheme of hybrid AC/DC system is chosen for demonstration, and the corresponding control parameters are shown in TABLE 5.

The convergence of unified method is set to $\varepsilon = 10^{-6}$, whilst the convergence criteria of sequential method is set as following: $\varepsilon_{ac} = \varepsilon_{dc} = 10^{-6}$. Employing the proposed unified algorithm, the power flow converges in 6 iterations. However, the reactive power of VSC2 is $Q_{s2} = -0.6368$ p.u. and it exceeds the preset lower limit $-Q_{s\max 2} = -0.4898$p.u.

TABLE 5. Master-slave control scheme of the hybrid AC/DC system.

Station		Capacity S_N/p.u.	D-axis control	Q-axis control	E-axis control
VSC	1	0.7	$U_{dc1}^* = 1.0$	$Q_{s1}^* = 0$	/
	2	0.7	$P_{s2}^* = 0.5$	$U_{s2}^* = 1.0$	/
LCC	3	2.5	$P_{dc3}^* = 0.8$	/	$T_3^* = 0.9$

TABLE 6. Validation results for the hybrid AC/DC system.

Bus	Unified method		Sequential method	
	V_{ac} /p.u.	δ_{ac} /rad	V_{ac} /p.u.	δ_{ac} /rad
1	1.0600	0	1.0600	0
2	1.0450	-0.0886	1.0450	-0.0886
3	1.0100	-0.2241	1.0100	-0.2241
4	1.0107	-0.1793	1.0107	-0.1793
5	1.0119	-0.1581	1.0119	-0.1580
6	1.0700	-0.3552	1.0700	-0.3551
7	1.0423	-0.2170	1.0423	-0.2169
8	1.0900	-0.2170	1.0900	-0.2169
9	1.0177	-0.2370	1.0177	-0.2369
10	1.0194	-0.2633	1.0194	-0.2632
11	1.0407	-0.3110	1.0407	-0.3109
12	1.0507	-0.3620	1.0507	-0.3619
13	1.0450	-0.3536	1.0450	-0.3535
14	1.0099	-0.3067	1.0099	-0.3066
Variables	Unified method		Sequential method	
U_{f2} /p.u.	0.9724		0.9724	
δ_{f2} /rad	-0.1850		-0.1849	
U_{dc1} /p.u.	1.0000		1.0000	
U_{dc2} /p.u.	1.0026		1.0026	
U_{dc3} /p.u.	1.0077		1.0077	
$\cos\theta$	0.8623		0.8623	
$\cos\varphi$	0.7787		0.7787	
Comp. time	0.015 s		0.055 s	

according to (50). Therefore, the Q-axis control mode of VSC2 should be changed to constant reactive power $Q_{s2}^* = -Q_{s\max 2}$; meanwhile, the LCC over-limitation is taken into account as well, due to its unusual over-limitation, there is no switching control modes occur in LCC in this test. The results are shown in TABLE 6.

It can be investigated from the TABLE 6 below that the results of unified method are basically consistent with the results of sequential method. The only slight difference between them lies in the AC bus phase angle, and the results of DC parameters are absolutely consistent. This is due to that the processing modes of converter power flow for unified method and sequential method are different, which causes a little difference in the results of AC grid. In the meantime, the computing time shows that the unified method is approximately four times faster than the sequential method, what's more, the unified method possesses a very good convergence in such complex power flow calculation. From the analysis above, it reveals that the proposed unified method is valid

TABLE 7. Convergence of different operating cases.

Times of load growth	0.1	0.5	1.0	1.5	2.0	2.5	3.0	3.5	4.0
Times of iteration	9	9	9	9	9	11	13	15	25

TABLE 8. Droop control scheme of the hybrid AC/DC system.

Station		Capacity S_N/p.u.	D-axis control	Q-axis control	E-axis control
VSC	1	0.7	Droop	$Q_{s1}^* = 0$	/
	2	0.7	Droop	$Q_{s2}^* = 0.1$	/
LCC	3	2.5	$P_{dc3}^* = 0.8$	/	$T_3^* = 0.9$

and efficient. Owing to these features, the proposed unified method is more suitable for probabilistic power flow calculation and online stead-state security assessment for such hybrid AC/DC system particularly incorporating with LCC and VSC.

2) ROBUSTNESS OF THE PROPOSED DPF ALGORITHM

In order to verify the robustness of the proposed hybrid AC/DC power flow algorithm, the following experiment is conducted based on case a), in which the load condition is changed via increasing the ratio of all AC/DC loads from 0.1 to 4.0 times, which indicates the robustness of the algorithm in different stressed cases. The detailed results of this experiment are shown as below.

It can be investigated from the TABLE 7 that the proposed hybrid AC/DC power flow algorithm possess good robustness even under stressed cases. Before two times of load growth, the convergence keeps invariant. As the load further increases, the times of iteration increase slowly, when the load growth come up to four times, the number of iteration increases dramatically. The test results validate the good robustness of the proposed hybrid AC/DC power flow calculation algorithm in both light and heavy load conditions.

3) UNIVERSALITY OF THE PROPOSED DPF ALGORITHM

Usually, there are three control schemes in HVDC systems including master-slave control, voltage margin control and voltage droop control. Master-slave control scheme is validated in case a), while voltage margin control can be regarded as a special form of master-slave control. In order to verify the universality of the proposed hybrid AC/DC algorithm in a further step, the droop control scheme is selected herein for demonstration.

The parameters of droop control can be preset to: $K_{U-P,1} = K_{U-P,2} = 0.04$, $U_{dc1}^* = 1.005$, $P_{dc1}^* = 0.55$, $U_{dc2}^* = 0.995$, $P_{dc2}^* = 0.25$. The test results of such operating mode are given below.

Under droop control scheme, the two VSC stations both work in droop control mode, forming multi-slack bus for

TABLE 9. Power flow calculation results of droop control.

Station	P_{dc}/p.u.	U_s/p.u.	P_s/p.u.	P_{loss}/p.u.	Loss Rate/%
1	0.3732	1.0188	0.3632	0.0096	2.64
2	0.4214	1.0812	0.4113	0.0097	2.36
3	0.8000	1.0700	0.8014	0.0014	0.175
U_{dc1}/p.u.	0.9979		$\cos\theta$	0.8617	
U_{dc2}/p.u.	1.0019		$\cos\varphi$	0.7780	
U_{dc3}/p.u.	1.0068		Comp. time	0.0180 s	

DC grid. Together with the results in Section VI.A a), the test results in TABLE 9 indicate that the proposed unified method can deal with power flow calculation for multiple control modes of such hybrid AC/DC system and possesses a good universality. What's more, the proposed unified method only needs a little computing time which entails a very high efficiency and convergence. Meanwhile, as seen from the TABLE 9, the power loss of VSC station approximately accounts for 2% of the transmission power. Therefore, it is vital to take the precise model of station into account, otherwise, it will bring an adverse impact on the accuracy of the calculation and economic dispatch. Besides, the power loss of LCC station is much less than the one of VSC station.

B. PROBABILISTIC POWER FLOW ANALYSIS FOR HYBRID AC/DC SYSTEM BASED ON LHS AND NATAF TRANSFORMATION

In this sub-section, the computational accuracy and effectiveness of the proposed PPF for hybrid HVAC and LCC-VSC will be evaluated considering the correlation of various random variables subject to the different types of probability distributions. In addition, the probabilistic interactions amongst the LCC stations and VSC stations as well as the effects of uncertainties on the operating control schemes are investigated with numerical simulations.

As shown in Fig. 5, the test system is a modified IEEE 118-bus system including a LCC and VSC based hybrid AC/MTDC grid employed for photovoltaic (PV_1, PV_2) plant integration in the main grid, a pure VSC-MTDC used for wind farm WF_{-1} connected to the AC grid and three two-terminal LCCs embedded in the AC grid. The other two wind farms WF_2 and WF_3, and a photovoltaic (PV_3) plant are directly connected to the AC bus 12, bus 103 and bus 59 respectively. The capacity is set to 200 MW, 85 MW, 40 MW, 120 MW, 140 MW, 155 MW for WF_1, WF_2, WF_3, PV_1, PV_2, PV_3, respectively.

The corresponding control schemes of hybrid LCC-VSC converter stations are shown in TABLE 10, where the specific parameters of droop control are given as: $K_{U-P,1} = K_{U-P,2} = 0.04$, $U_{dc1}^* = 1.005$, $P_{dc1}^* = 1.05$, $U_{dc2}^* = 0.995$, $P_{dc2}^* = 0.65$. In addition, the pure VSC-MTDC and pure LCCs control schemes are shown in TABLE 11 and TABLE 12, separately.
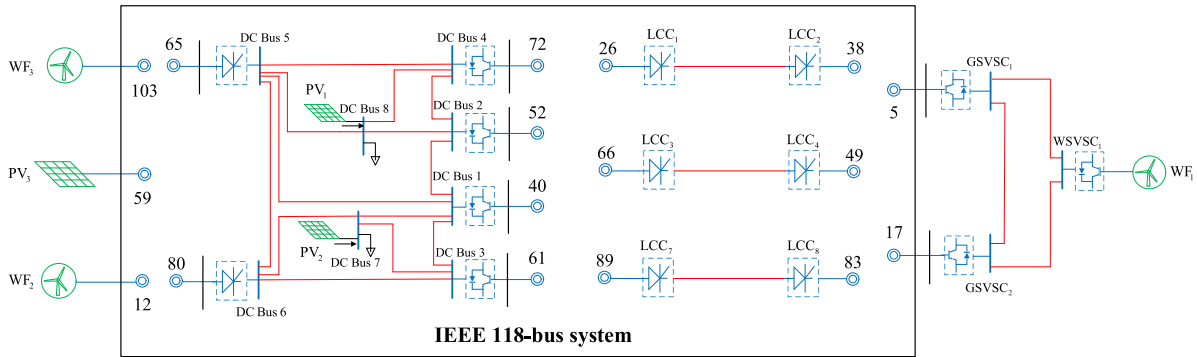
FIGURE 5. Modified IEEE 118-bus system with hybrid AC/DC grid incorporating both LCC and VSC.

TABLE 10. Control scheme of LCC and VSC in hybrid AC/DC system.

Station		D-axis control	Q-axis control	E-axis control
VSC	1	Droop	$Q_{s1}^* = 0$	/
	2	Droop	$Q_{s2}^* = 0.1$	/
	3	$P_{s3}^* = 1.8$	$Q_{s3}^* = 0$	/
	4	$P_{s4}^* = 1.5$	$Q_{s4}^* = 0$	/
LCC	5	$P_{dc5}^* = 1.8$	/	$T_5^* = 1.025$
	6	$P_{dc6}^* = 1.6$	/	$T_6^* = 0.95$

TABLE 11. Control schemes of AC/VSC-MTDC system.

	$GSVSC_1$	$GSVSC_2$	$WSVSC_1$
Control modes	$U_{dc1} - Q_{s1}$	$P_{s2} - Q_{s2}$	DMCS
Control parameters	$U_{dc1}^* = 1.0$	$P_{s2}^* = 1.2$	$U_{s3}^* = 1.02$
	$Q_{s1}^* = 0$	$Q_{s2}^* = 0.1$	

TABLE 12. Control scheme of two-terminal LCC system.

	LCC_1	LCC_2	LCC_3
Control parameters	$P_{dc1}^* = 1.5$	$U_{dc2}^* = 1.02$	$P_{dc3}^* = 1.6$
	$T_{LCC1}^* = 1.025$	$T_{LCC2}^* = 0.95$	$T_{LCC3}^* = 1.025$
	LCC_4	LCC_7	LCC_8
Control parameters	$U_{dc4}^* = 1.02$	$P_{dc7}^* = 1.2$	$U_{dc8}^* = 1.03$
	$T_{LCC4}^* = 0.975$	$T_{LCC7}^* = 1.025$	$T_{LCC8}^* = 0.95$

TABLE 13. Probability distribution of uncertainty sources.

Type	CDF	Parameter1	Parameter2
Weibull	$1 - \exp\left(-(\frac{x}{D})^k\right)$	0.1105 (load)	2.3302 (load)
		7.2108 (wind)	1.8370 (wind)
Normal	$\int_{-\infty}^{x} \frac{1}{\sqrt{2\pi}\sigma} \exp\left(-\frac{(x-\mu)^2}{2\sigma^2}\right) dx$	Depends on the specific loads	
Uniform	$\int_a^x \frac{1}{b-a} dx$	Depends on the specific loads	
Beta	$\frac{\Gamma(K+M)}{\Gamma(K)\Gamma(M)} \int_0^x (x)^{K-1}(1-x)^{M-1} dx$	6.06	4.51

TABLE 14. Correlation coefficients of uncertainty sources.

	Load1	Load2	Load3	genWF	genPV
Load1	0.7	0.4	0.4	0.15	0
Load2	0.4	0.7	0.4	0.15	0
Load3	0.4	0.4	0.7	0.15	0
genWF	0.15	0.15	0.15	0.8	-0.2
genPV	0	0	0	-0.2	0.8

In details, the CDFs of these distributions are listed in TABLE 13.

The Pearson correlation coefficients across the five groups are set as shown in TABLE 14. Note that the random variables in **Load1**, **Load2** and **Load3** represent directly the corresponding loads. The random variables of **genWF** and **genPV** are given in term of wind speed (m/s) and solar radiation (MW/m²), which can be converted to power according to [33]. In TABLE 14, the non-diagonal elements represent the inter-group correlation; on the other hand, the diagonal elements denote intra-group correlation, looking into which the correlation coefficient of each variable itself is equal to one.

In order to illustrate the efficiency and accuracy of the proposed method, the MCS method based on crude random samples is applied to work as the reference. The sample size

In the test system, there are 99 loads in total in AC grid, which can be divided into three groups, load1 to load 59 are defined as **Load1** which follow Normal distribution with a standard deviation equaling to 5% of the mean value; load 60 to load 79 are treated as **Load2** which follow Uniform distribution; load 80 to load 99 are denoted by **Load3** which follow Weibull distribution. In addition, all wind farms are subject to Weibull distribution as well (denoted by **genWF**), and all PVs follow Beta distribution (denoted by **genPV**). Thus, there are totally 105 random variables discussed herein.

TABLE 15. The errors of mean deviation of variables for AC system.

Variables	The average-mean error / %			
	PEM-(2m+1)	LHS-(2m+1)	LHS-1000	LHS-10000
U_{bus-ac}	0.0018	0.0044	0.0015	0.0003453
δ_{bus-ac}	0.2603	0.6046	0.1100	0.0832
$P_{Line-ac}$	1.1082	2.0527	0.4829	0.2788
$Q_{Line-ac}$	1.9516	1.7226	0.7657	0.2563

FIGURE 6. Comparison in the standard deviation errors.

(a). AC bus voltage magnitudes

(b). AC bus voltage phase angles

(c). Active power of the branch

(d). Reactive power of the branch

FIGURE 7. Comparison in the standard deviation errors.

(a). DC bus voltage

(b). Active power of the DC branch

of 50000 is sufficient enough to yield reliable estimates of the means and standard deviations. In addition, the Nataf transformation in combination with point estimate method (PEM) [34] is employed for comparison.

1) PERFORMANCE ASSESSMENT OF THE PROPOSED PPF

Considering the high dimensionality of random variables involved for hybrid AC/DC grid with increasing complexity and nonlinearity of the model, LHS-MCS method and the approximate method PEM in terms of $2m+1$ are adopted to conduct the PPF. LHS-MCS utilizes $2m+1$ samples, 1000 samples and 10000 samples, respectively, for comparison, in which m denotes the number of random variables and it is set to 105 for this test, thus $2m+1$ is equal to 211. The results of AC bus voltage magnitudes, phase angles, active power and reactive power of branches are shown below.

It can be investigated from the TABLE 15 that the average-mean errors for each type of target random outputs obtained by the four methods are small. All of the four methods have a good accuracy in mean value. However, in terms of the standard deviation error, the PEM method is obviously not applicable for probabilistic power flow analysis of hybrid AC/DC system any more. Seen from the figures below, the standard deviation error of PEM is very large, meanwhile, it suffers from sharp violation for some voltage magnitudes and reactive powers, it is mainly arisen by that the relevant nodes are connected or close to the converter station and renewable energy sources. These devices have adverse effects on the accuracy of the PEM. In principle, PEM method is poor for the high-order statistical moment estimation of target outputs. With the complexity and nonlinearity of the model increasing, the PEM method becomes incompetent. In contrast, the LHS-MCS method still performs well that the results of standard deviation error appears smooth; what's more, along with the sample size increasing, the accuracy for both mean error and standard deviation error is further improved significantly.

Similar to AC side, the average-mean errors of DC voltage are also very small, which are 0.042%, 0.1%, 0.005%, 0.0028% for PEM-(2m+1), LHS-(2m+1), LHS-1000, LHS-10000, respectively. The average-mean errors of DC branch active power obtained by these four methods are 0.37%, 0.9%, 0.18%, 0.028%, individually. These four methods have
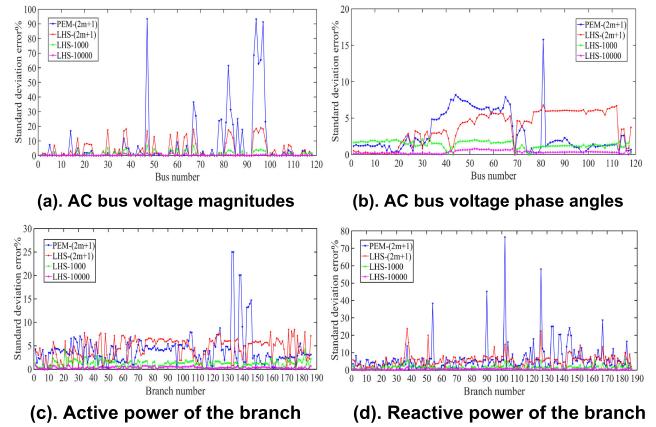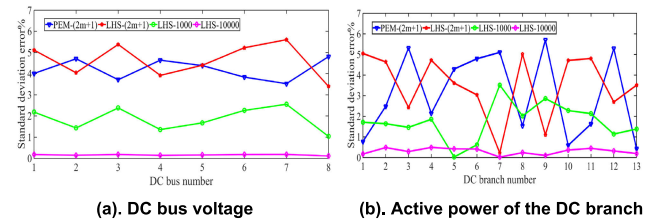
a good performance in the calculation for the mean of target random outputs in DC grid. However, the standard deviation errors for DC bus voltage and DC branch flow obviously increase. It can be observed from the Fig. 7 that the PEM and LHS with the same sample size have nearly identical error; nevertheless, with the sample size increasing, the standard deviation error of LHS method will decrease remarkably, in specific it is able to maintain the ones for all the DC variables under 5%.

Overall, the uncertainties for renewable energy sources integrated in main grid considering correlation and different distributions will impose only slight impact on the mean values, while they have a significant effect on the standard deviation of outputs; moreover, the uncertainties have a little impact on bus voltage magnitude, while the voltage phase angle and branch flow are affected greatly. In terms of accuracy property, as one of approximate methods the PEM is not applicable for probabilistic power flow analysis of new hybrid AC/DC system any more, although the PEM method needs only a few sample points for high efficiency and it is used widely in pure AC system. By contrast, the traditional LHS-MCS have a robust performance even with the sample size changing. From the results above, it discloses that LHS-1000 and LHS-10000 achieve a good accuracy for all the target outputs, which performs very steadily with all the errors below 5%. However, a tradeoff needs to be made between the accuracy and efficiency in practical operation. The calculation time for these four methods are 47.168 s, 47.339 s, 222.042 s, 2286.870 s. From the results of calculation time, it indicates that LHS-1000 can complete the PPF of hybrid
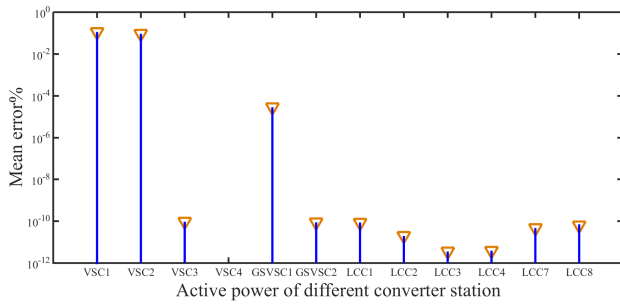
FIGURE 8. Probabilistic interactions on mean error for different converter stations.
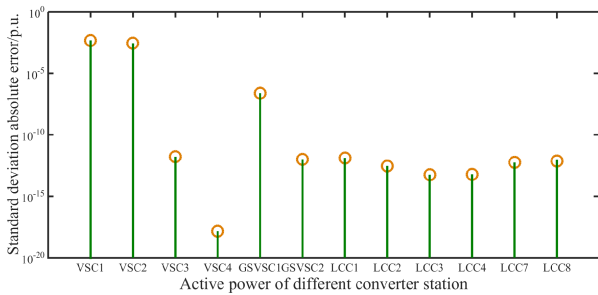

FIGURE 9. Probabilistic interactions on standard deviation error for different converter stations.

AC/DC grids within 5 minutes, while the LHS-10000 needs to consume about 38 minutes which is unacceptable in practical operation. To summarize, LHS-1000 does not only guarantee a good accuracy but also possess a high efficiency, therefore, LHS-1000 is adopted to conduct the PPF of hybrid AC/DC grids in the subsequent tests and analysis.

2) ACCURACY AND ROBUSTNESS OF PROPOSED PPF

The computational accuracy and robustness of the proposed method will be evaluated in this sub-section, under the impact of different correlation levels of random input variables, diverse fluctuation ranges of loads and different scales of random input variables.

a: PERFORMANCE EVALUATION WITH DIFFERENT CORRELATION LEVELS

The correlations between wind speeds, solar radiations, and loads are non-negligible in modern power systems. Thus, the complex PPF for hybrid AC/DC grids is desirable. In order to evaluate the performance of the proposed method, seven scenarios are designed below: the correlation coefficient matrix are set to be $0 \times C_R$, $0.2 \times C_R$, $0.4 \times C_R$, $0.6 \times C_R$, $0.8 \times C_R$, $1 \times C_R$, $1.2 \times C_R$, respectively.

Table 16 presents the maximum and average errors of means and standard deviations (STD) of state variables with different correlation coefficients. The results above turn out that the errors of all state variables are lower than 5%, which entails the good accuracy and robustness of LHS-1000 with respect to handling various correlation levels for complex hybrid AC/DC system.

TABLE 16. The errors of mean and standard deviation of state variables.

Target variable	Max-Mean error %	Average-Mean error %	Max-STD error %	Average-STD error %
U_{ac}	0.99	0.0197	4.61	0.64
δ_{ac}	0.97	0.0721	4.80	1.56
U_{dc}	0.0246	0.0093	1.70	1.08

TABLE 17. The errors of mean and standard deviation of state variables.

Fluctuation ranges	The average errors % of U_{ac}		The average errors % of δ_{ac}		The average errors % of U_{dc}	
	Mean	STD	Mean	STD	Mean	STD
15%	0.01951	0.47	0.0532	1.36	0.00403	0.59
20%	0.01965	0.52	0.0610	1.55	0.00658	0.62
25%	0.01976	0.59	0.0640	1.73	0.00817	0.77
30%	0.01982	0.68	0.0811	2.06	0.01280	1.43

b: PERFORMANCE EVALUATION WITH DIFFERENT FLUCTUATION RANGES OF LOADS

In order to further evaluate the computational accuracy and robustness of the proposed method even in more severe operation scenarios of the hybrid HVAC and LCC-VSC system, the fluctuation range of each load is set to 15%, 20%, 25%, and 30% of its mean value, respectively.

As shown in TABLE 17, with the fluctuation ranges of loads increasing, the average errors of all state variables are lower than 3%, which verifies superior accuracy and robustness of LHS-1000. Meanwhile, it can be investigated that with the volatility of loads become larger, the average errors of AC voltage, AC phase angle and DC voltage have a slowly increasing tendency. Moreover, the errors in DC voltage increase more dramatically.

c: PERFORMANCE EVALUATION WITH DIFFERENT SCALES OF RANDOM INPUT VARIABLES

In order to identify the influence on different scales of random input variables, the following four test scenarios are designed: scenario **S1** includes **genWF** and **genPV** with 6 random inputs, scenario **S2** includes **S1** and **Load1** with 65 random inputs, **S3** includes **S2** and **Load2** with 85 random inputs, **S4** includes **S3** and **load3** with 105 random inputs.

It can be observed from the TABLE 18 that with the uncertain capacities and uncertain random variables increasing, the maximum and average errors of all state variables also rise up slowly. However, LHS-1000 can also maintain a good accuracy and robustness in dealing with diverse scenarios with different numbers of random inputs.

TABLE 18. The errors of standard deviation of state variables.

Scenario	U_{ac}		δ_{ac}		U_{dc}	
	Max-STD error %	Average-STD error %	Max-STD error %	Average-STD error %	Max-STD error %	Average-STD error %
S1	2.88	0.36	1.14	0.46	0.24	0.20
S2	3.42	0.44	1.65	0.77	0.36	0.33
S3	3.84	0.49	3.28	1.24	0.86	0.66
S4	4.04	0.64	3.74	1.81	1.51	1.17

3) PROBABILISTIC INTERACTIONS BETWEEN CONVERTER STATIONS AND CONTROL SCHEMES

The following figures show the probabilistic interactions on accuracy of active power for different converter stations with various control schemes, in which, VSC1 and VSC2 adopt droop control, VSC3 and VSC4 are in terms of constant active power control; GSVSC1 takes constant DC voltage control, GSVSC2 is in a constant active power control, while LCC conveter utilizes constant active power and DC voltage, respectively, for two-terminal system.

It can be investigated from the figures above that probabilistic interactions on means and standard deviation have the same general tendency. Overall, the probabilistic characteristics of uncertainty sources have greater effects on VSC station than LCC station in terms of accuracy. This is since that the LCC is not able to control the active and reactive power separately and flexibly as the VSC station, and the corresponding power flow calculation of converter station is simpler, so the active power of LCC station is more stable and less susceptible to probability fluctuations. For VSC stations, it can be investigated from the figures above that the probabilistic characteristics have the largest impact on droop control, and the constant DC voltage control VSC station takes the second place, the constant active power control station is least affected. This is owing to the fact that the active power balance is affected by both AC grid and DC grid under droop control, in addition, the active power and DC voltage are both unknown variables. However, in constant DC voltage control mode, the active power is the only one unknown variable, and it is just affected by DC grid, these reasons together lead to the constant DC voltage control be slightly affected by the probabilistic characteristics, and the results obtained under a constant active power control are relatively steady. In the remaining test, the focus will be put on the interaction of probabilistic characteristics with the droop control.

Four operation scenarios are designed and set with different droop coefficients, which are 0.1, 0.07, 0.04, and 0.02, respectively. The results of four operation scenarios for DC side and AC are shown in Fig.10 and Fig.11. It can be investigated from the Fig.11 that with the droop coefficient increasing, the risk of the DC voltage beyond the lower limitation is also becoming higher. The further research finds
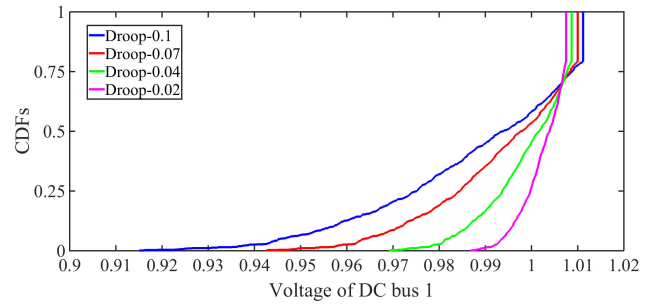

FIGURE 10. CDFs of different droop coefficients for voltage of DC bus 1 with droop control.
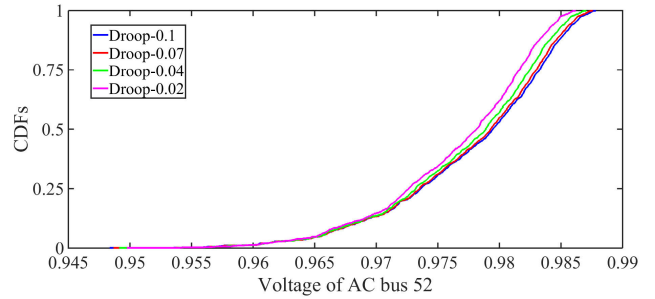

FIGURE 11. CDFs of different droop coefficients for voltage of AC bus 52 connected to droop control VSC1 station.

that with the droop decreasing, the power flow convergence issue is getting harder: when the droop coefficient reaches at 0.01, the whole system suffers from non-convergence. It is mainly due to that when droop coefficient tends to zero, the DC grid has two constant DC voltage control, that is to say, there are two slack buses in DC grid which leads to non-convergence. Therefore, the droop coefficient should have a reasonable scope which is not too large or too small. In specific, it can be investigated that the droop coefficient between 0.03 and 0.07, the whole hybrid HVAC and LCC-VSC system can achieve a good balance between security and convergence in this test system. Moreover, probability distribution of DC voltage is also changed to non-normal distribution with adoption of droop control, since there is existing an upper limitation in DC voltage. Compared to DC side, the different droop coefficients bring a slight impact on AC voltage magnitude as seen from Fig.11.

VII. CONCLUSION

This paper establishes a unified approach to DPF, and in a further step PPF analysis based on a combination of Nataf transformation and LHS, for a new hybrid AC/DC system incorporating VSC, LCC and the correlated various uncertainty sources.

A modified IEEE 14-bus system is taken to validate the effectiveness and universality of the unified deterministic power flow approach for hybrid AC/DC system; in addition, a PPF analysis for hybrid AC/DC system is tested on a modified IEEE 118-bus system. The major conclusions can be summarized in what follows:

1) The proposed unified DPF approach considering precise model of converter and coordinated control is

effective to calculate the power flow of hybrid AC/DC grids incorporating both LCC and VSC converters even under different operation modes.

2) As the deterministic model become more complex, the PEM method is not applicable for PPF analysis of hybrid AC/DC system any more. Compared with the PEM method, the LHS-MCS is more efficient with high accuracy. Based on the simulation results, LHS-1000 method achieves a good performance in holding a balance amongst accuracy, efficiency and robustness for practical operation.

3) The impacts of probabilistic characteristics arisen from the uncertainty sources on different types of converter and control schemes are investigated in this paper. It shows that LCC converter is less affected by the uncertain factors, while for VSC converter with the droop control it suffers from a significant influence. Based on further research, it reveals that the droop coefficients setting should satisfy a proper range which is not too large or too small.

REFERENCES

[1] L.-Q. Liu and C.-X. Liu, "VSCs-HVDC may improve the electrical grid architecture in future world," *Renew. Sustain. Energy Rev.*, vol. 62, pp. 1162–1170, Sep. 2016.

[2] *Eu Energy Policy to 2050: Achieving 80%-95% Emission Reductions*, Eur. Wind Energy Assoc., Brussels, Belgium, 2011.

[3] G.-D. Wang, R.-J. Wai, and Y. Liao, "Design of backstepping power control for grid-side converter of voltage source converter-based high-voltage dc wind power generation system," *IET Renew. Power Gener.,*, vol. 7, no. 2, pp. 118–133, Mar. 2013.

[4] R. Li, S. Bozhko, and G. Asher, "Frequency control design for offshore wind farm grid with LCC-HVDC link connection," *IEEE Trans. Power Electron.*, vol. 23, no. 3, pp. 1085–1092, May 2008.

[5] N. Flourentzou, V. G. Agelidis, and G. D. Demetriades, "VSC-based HVDC power transmission systems: An overview," *IEEE Trans. Power Electron.*, vol. 24, no. 3, pp. 592–602, Mar. 2009.

[6] D. Van Hertem and M. Ghandhari, "Multi-terminal VSC HVDC for the European supergrid: Obstacles," *Renew. Sustain. Energy Rev.*, vol. 14, no. 9, pp. 3156–3163, Dec. 2010.

[7] T. M. Haileselassie and K. Uhlen, "Power system security in a meshed north sea HVDC grid," *Proc. IEEE*, vol. 101, no. 4, pp. 978–990, Apr. 2013.

[8] J. Liao, N. Zhou, Q. Wang, C. Li, and X. Huang, "VSC-HVDC fault clearing strategy based on parallel LCC shunting and inverse voltage suppression," *High Voltage Eng.*, vol. 45, no. 1, pp. 63–71, Jan. 2019.

[9] J. Lei, T. An, Z. Du, and Z. Yuan, "A general unified AC/DC power flow algorithm with MTDC," *IEEE Trans. Power Syst.*, vol. 32, no. 4, pp. 2837–2846, Jul. 2017.

[10] C. M. Ong and A. Hamzei-nejad, "A general-purpose multiterminal DC load-flow," *IEEE Trans. Power App. Syst. (through 1985)*, vols. PAS-100, no. 7, pp. 3166–3174, Jul. 1981.

[11] T. Smed, G. Andersson, G. B. Sheble, and L. L. Grigsby, "A new approach to AC/DC power flow," *IEEE Trans. Power Syst.*, vol. 6, no. 3, pp. 1238–1244, Aug. 1991.

[12] M. M. El-marsafawy and R. M. Mathur, "A new, fast technique for load-flow solution of integrated multi-terminal DC/AC systems," *IEEE Trans. Power App. Syst. (through 1985)*, vols. PAS-99, no. 1, pp. 246–255, Jan. 1980.

[13] C. Liu, B. Zhang, Y. Hou, F. F. Wu, and Y. Liu, "An improved approach for AC-DC power flow calculation with multi-infeed DC systems," *IEEE Trans. Power Syst.*, vol. 26, no. 2, pp. 862–869, May 2011.

[14] J.-C. Fernández-Pérez, F. M. E. Cerezo, and L. R. Rodríguez, "On the convergence of the sequential power flow for multiterminal VSC AC/DC systems," *IEEE Trans. Power Syst.*, vol. 33, no. 2, pp. 1768–1776, Mar. 2018.

[15] J. Beerten, S. Cole, and R. Belmans, "Modeling of multi-terminal VSC HVDC systems with distributed DC voltage control," *IEEE Trans. Power Syst.*, vol. 29, no. 1, pp. 34–42, Jan. 2014.

[16] W. Wang and M. Barnes, "Power flow algorithms for multi-terminal VSC-HVDC with droop control," *IEEE Trans. Power Syst.*, vol. 29, no. 4, pp. 1721–1730, Jul. 2014.

[17] J. Beerten, S. Cole, and R. Belmans, "Generalized steady-state VSC MTDC model for sequential AC/DC power flow algorithms," *IEEE Trans. Power Syst.*, vol. 27, no. 2, pp. 821–829, May 2012.

[18] J. Arrillaga and P. Bodger, "Integration of h.v.d.c. links with fast-decoupled load-flow solutions," *Proc. Inst. Elect. Eng.*, vol. 124, no. 5, pp. 463–468, May 1977.

[19] R. Chai, B. Zhang, J. Dou, Z. Hao, and T. Zheng, "Unified power flow algorithm based on the NR method for hybrid AC/DC grids incorporating VSCs," *IEEE Trans. Power Syst.*, vol. 31, no. 6, pp. 4310–4318, Nov. 2016.

[20] J. Reeve, G. Fahny, and B. Stott, "Versatile load flow method for multiterminal HVDC systems," *IEEE Trans. Power App. Syst.*, vol. PAS-96, no. 3, pp. 925–933, May 1977.

[21] M. Baradar and M. Ghandhari, "A multi-option unified power flow approach for hybrid AC/DC grids incorporating multi-terminal VSC-HVDC," *IEEE Trans. Power Syst.*, vol. 28, no. 3, pp. 2376–2383, Aug. 2013.

[22] Y. Wei, Q. He, Y. Sun, Y. Sun, and C. Ji, "Improved power flow algorithm for VSC-HVDC system based on high-order newton-type method," *Math. Problems Eng.*, vol. 2013, 2013, Art. no. 235316.

[23] B. Borkowska, "Probabilistic load flow," *IEEE Trans. Power App. Syst.*, vol. PAS-93, no. 3, pp. 752–759, May 1974.

[24] S. Peng, J. Tang, and W. Li, "Probabilistic power flow for AC/VSC-MTDC hybrid grids considering rank correlation among diverse uncertainty sources," *IEEE Trans. Power Syst.*, vol. 32, no. 5, pp. 4035–4044, Sep. 2017.

[25] Z. Zhu, S. Lu, and S. Peng, "An improved stochastic response surface method based probabilistic load flow for studies on correlated wind speeds in the AC/DC grid," *Energies*, vol. 11, no. 12, p. 3501, 2018.

[26] P. Zhang and S. T. Lee, "Probabilistic load flow computation using the method of combined cumulants and Gram-Charlier expansion," *IEEE Trans. Power Syst.*, vol. 19, no. 1, pp. 676–682, Feb. 2004.

[27] J. M. Morales, L. Baringo, A. J. Conejo, and R. Mínguez, "Probabilistic power flow with correlated wind sources," *IET Gener., Transmiss. Distrib.*, vol. 4, no. 5, pp. 641–651, May 2010.

[28] M. Aien, M. Fotuhi-Firuzabad, and F. Aminifar, "Probabilistic load flow in correlated uncertain environment using unscented transformation," *IEEE Trans. Power Syst.*, vol. 27, no. 4, pp. 2233–2241, Nov. 2012.

[29] Y. Chen, J. Wen, and S. Cheng, "Probabilistic load flow method based on Nataf transformation and latin hypercube sampling," *IEEE Trans. Sustain. Energy*, vol. 4, no. 2, pp. 294–301, Apr. 2013.

[30] H. Yu, C. Y. Chung, K. P. Wong, H. W. Lee, and J. H. Zhang, "Probabilistic load flow evaluation with hybrid latin hypercube sampling and Cholesky decomposition," *IEEE Trans. Power Syst.*, vol. 24, no. 2, pp. 661–667, May 2009.

[31] A. Gómez-Expósito, A. J. Conejo, and C. Cañizares, *Electric Energy Systems: Analysis and Operation*. Boca Raton, FL, USA: CRC Press, 2009.

[32] Q. Xiao, "Evaluating correlation coefficient for Nataf transformation," *Probabilistic Eng. Mech.*, vol. 37, pp. 1–6, Jul. 2014.

[33] H. R. Baghaee, M. Mirsalim, G. B. Gharehpetian, and H. A. Talebi, "Fuzzy unscented transform for uncertainty quantification of correlated wind/PV microgrids: Possibilistic–probabilistic power flow based on RBFNNs," *IET Renew. Power Gener.*, vol. 11, no. 6, pp. 867–877, May 2017.

[34] Y. Li, W. Li, W. Yan, J. Yu, and X. Zhao, "Probabilistic optimal power flow considering correlations of wind speeds following different distributions," *IEEE Trans. Power Syst.*, vol. 29, no. 4, pp. 1847–1854, Jul. 2014.
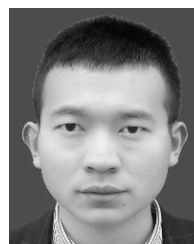
TONG SHU (S'18) was born in Hubei, China, in 1995. He received the B.S. degree in electric engineering from Guizhou University, Guizhou, China, in 2017. He is currently pursuing the M.S. degree with the School of Electric Engineering, Chongqing University, Chongqing, China. His current research interests include modeling of hybrid AC/DC systems, probabilistic power flow algorithms, dynamic power flow, and uncertainty analysis in power systems.

XINGYU LIN (S'18) was born in Chongqing, China, in 1994. He is currently pursuing the Ph.D. degree with the School of Electrical Engineering, Chongqing University, Chongqing. His current research interests include probabilistic modeling of uncertainty sources in power systems, advanced probabilistic power flow method, and neural network algorithms.

FENG LI was born in Guangdong, China, in 1980. He received the Ph.D. degree from the School of Electric Power Engineering, South China University of Technology, Guangzhou, China. He is currently a Senior Engineer with the Grid Planning and Research Center, Guangdong Power Grid Corporation, China Southern Power Grid Company Limited. His current research interests include power system planning and economical operation of the power systems.

SUI PENG was born in Jiangxi, China, in 1992. He received the M.S. degree from the School of Electrical Engineering, Chongqing University, Chongqing, China. He is currently an Assistant Engineer with the Grid Planning and Research Center, Guangdong Power Grid Corporation, China Southern Power Grid Company Limited. His current research interests include transmission system risk assessment and advanced probabilistic power flow method. He was a recipient of the International PMAPS Roy Billinton Student Paper Silver Award, in 2016.

JUNJIE TANG (M'14) received the Ph.D. degree in electrical engineering from the E.ON Energy Research Center, Institute for Automation of Complex Power Systems, RWTH Aachen University, Aachen, Germany, in 2014. He is currently an Associate Professor with the State Key Laboratory of Power Transmission Equipment and System Security and New Technology, Power and Energy Reliability Research Center, School of Electrical Engineering, Chongqing University, Chongqing, China. His current research interests include power system uncertainty quantification analysis, power system security risk assessment and optimal management, and modeling of hybrid AC/DC grid.

XIAO DU received the B.S. degree from the School of Electrical Engineering, Shandong University, Jinan, China, in 2018. He is currently pursuing the M.S. degree with the School of Electrical Engineering, Chongqing University, Chongqing, China. His current research interests include optimal operation and uncertainty analysis of power systems.

HUIXIANG CHEN was born in Guangdong, China, in 1963. He received the Ph.D. degree from the Department of Electrical Engineering, Tsinghua University, Beijing, China. He is currently a Senior Engineer (Professor Level) with the Grid Planning and Research Center, Guangdong Power Grid Corporation, China Southern Power Grid Company Limited. His current research interests include advanced dc transmission technology, power system planning, and economical operation of the power systems.

WENYUAN LI received the degree from Tsinghua University, Beijing, China, in 1968, and the M.S. and Ph.D. degrees from Chongqing University, Chongqing, China, in 1982 and 1987, respectively, all in electrical engineering, where he is currently a Professor. Dr. Li is a Foreign Member of the Chinese Academy of Engineering and a Fellow of the Canadian Academy of Engineering. He was a recipient of several awards, including the IEEE Power Engineering Society Roy Billinton Power System Reliability Award, in 2011, the International PMAPS Merit Award, in 2012, and the IEEE Canada Power Medal, in 2014. He served as an Editor for the IEEE TRANSACTIONS ON POWER SYSTEMS.

• • •